NACA

RESEARCH MEMORANDUM

THE INFLUENCE OF IMPERFECT RADAR SPACE STABILIZATION ON THE FINAL ATTACK PHASE OF AN AUTOMATIC INTERCEPTOR SYSTEM

By William C. Triplett, John D. McLean, and John S. White

Ames Aeronautical Laboratory
Moffett Field, Calif.

NATIONAL ADVISORY COMMITTEE FOR AERONAUTICS

WASHINGTON

March 11, 1957

NACA RM A56K19

NATIONAL ADVISORY COMMITTEE FOR AERONAUTICS

RESEARCH MEMORANDUM

THE INFLUENCE OF IMPERFECT RADAR SPACE STABILIZATION ON THE FINAL ATTACK PHASE OF AN AUTOMATIC INTERCEPTOR SYSTEM

By William C. Triplett, John D. McLean,
and John S. White

SUMMARY

The manner in which imperfect space stabilization of the tracking radar influences the flight path stability of an automatic interceptor during the attack phase is illustrated by means of flight and analog-computer time histories. It is shown analytically that these effects may be interpreted in terms of a destabilizing airplane rate feedback which can be canceled by an additional compensatory feedback in the radar tracking loop.

INTRODUCTION

As part of a general study of automatic flight control systems, the NACA is currently conducting a flight and analog-computer study of the final attack phase of an automatic interceptor system. The test vehicle chosen for these tests was an F-86D equipped with an automatic attack coupler (control surface tie-in), developed by the Hughes Aircraft Company, which tied the E-4 fire-control computer to the aircraft autopilot.

The primary purposes of this phase of the study are to develop adequate flight and simulation techniques and to determine the most promising areas for future research. A satisfactory correlation between flight and simulator results makes it possible to use the computer to examine a wide range of system modifications that may not be practical to test in flight.

This report presents some preliminary flight and simulator results in which lead-collision beam attacks were made against a nonmaneuvering target. The discussion is limited to results which illustrate the dominating influence of imperfect space stabilization of the radar

antenna on the tracking ability of the interceptor. Methods for alleviating these undesirable effects are considered. Also included as an appendix is a complete description of the system as simulated on the analog computer.

NOTATION

See Appendix A for definition of axes systems and orientation angles.

A	line-of-sight angle in azimuth, deg
A_a	antenna angle in azimuth, deg
A_j, A_k	components of desired acceleration proportional to S_j and S_k, respectively, g
A_{L_D}	desired lift acceleration (positive upward), g
A_Z	normal acceleration (positive downward), g
E	line-of-sight angle in elevation, deg
E_a	antenna angle in elevation, deg
F	desired target range at impact, ft
I	moment of inertia, slug-ft^2
M	Mach number
R	target range, ft
S	wing area, ft^2
S_j, S_k	azimuth and elevation steering signals, ft/sec, unless otherwise specified
T	time to go until impact, sec
V	relative velocity, $\overline{V}_B - \overline{V}_F$, ft/sec
V_B	target velocity, ft/sec
V_F	interceptor velocity, ft/sec
W	angular velocity of interceptor, radians/sec

[redacted]

b	wing span, ft
$\bar{c}$	mean aerodynamic chord, ft
m	mass, slugs
p	rolling velocity about body x axis, W_X, radians/sec
q	pitching velocity about body y axis, W_Y, radians/sec
r	yawing velocity about body z axis, W_Z, radians/sec
q_∞	dynamic pressure, $\frac{1}{2}\rho V_F^2$, lb/ft^2
s	differential operator, $\frac{d}{dt}$
t	time, sec
α	angle of attack, deg
β	angle of sideslip, deg
$\dot{\gamma}$	angular velocity of flight path, radians/sec
$\delta_a,\delta_H,\delta_r$	total aileron, stabilizer, and rudder deflections, respectively, radians
ϵ	tracking error angle of antenna, deg
ρ	air density, slugs/cu ft
Ω	angular velocity of target line of sight, radians/sec
ω	angular velocity of antenna, radians/sec
ω'	computed antenna rate signal, radians/sec
ψ,θ,φ	orientation angles of interceptor body axis system (see Appendix A)
$\psi_F,\theta_F,\varphi_F$	orientation angles of interceptor wind axis system (see Appendix A)
ψ_B,θ_B	orientation of target velocity vector

[redacted]

Subscripts

A	azimuth
E	elevation
ss	steady state

Axis Systems

X,Y,Z	interceptor wind axes
x,y,z	interceptor body axes
I,J,K	line-of-sight axes
i,j,k	antenna axes

TEST EQUIPMENT

The test vehicle used in the present investigation is a North American F-86D (shown in fig. 1) equipped with an E-4 fire-control system and an automatic attack coupler developed by the Hughes Aircraft Company. The complete system as shown in the schematic diagram of figure 2 consists of four primary elements: a self-tracking radar, attack computer, attack coupler, and the airplane-autopilot combination. These are described in more detail in the following paragraphs.

Radar

A block diagram of the radar with its geometric feedbacks is shown in figure 3. Here the elevation and azimuth channels are considered to function independently. Each channel contains a tracking loop consisting of the receiver (G_1) and a space stabilization loop containing the antenna drive motor (G_2) and the integrating rate gyro. The radar receiver senses the tracking error (ϵ_E in elevation) and supplies an antenna rate command ω_j' to the gyro. The voltage output of the gyro then drives the antenna to null the tracking error. In the steady state, the signal ω_j' is directly proportional to ϵ_E and exactly equal to ω_j; thus ω_j' is considered as the actual antenna rate for use in the computer.

[redacted]

The quantities $\dot{E}_a$ and $\dot{A}_a$ are the antenna gimbal rates relative to the airplane. The rate gyros mounted on the antenna sense the total angular rates of the antenna, and thus the inputs to the gyros are the sum of the gimbal rates and airplane angular rates expressed in the antenna coordinate system. These inputs may be written as

$$\omega_j = \dot{E}_a + W_j$$

and

$$\omega_k = \dot{A}_a \cos E_a + W_k$$

where the airplane angular velocities W_j and W_k are defined as

$$W_j = q \cos A_a - p \sin A_a$$

$$W_k = (p \cos A_a + q \sin A_a) \sin E_a + r \cos E_a$$

Thus it can be seen that the radar antenna is sensitive to interceptor motions as well as target line-of-sight rates.

The receiver (G_1) contains filtering and compensating networks, and the transfer functions shown at the bottom of figure 3 were determined from ground measurements. Similar methods were used to determine the transfer functions of the antenna drive G_2. The dynamic lag of the rate gyros was considered negligible.

Attack Computer

The computer was designed strictly for lead-collision rocket-firing attacks and mechanizes the following steering equations. These are derived in detail in reference 1 from the basic geometry of the lead-collision attack.

$$S_k = R\omega_j' + \frac{F}{T}\left(\cos A_a \sin E_a + J + \frac{D}{F}\right) \tag{1}$$

$$S_j = R\omega_k' + \frac{F}{T} \sin A_a \tag{2}$$

where

[redacted]

$$T = \frac{F \cos A_a \cos E_a - R}{\dot{R}} \qquad (3)$$

S_k and S_j are the elevation and azimuth steering signals; T is the time to go to impact; and F is a preset constant range at impact. The distance F is normally set at 1500 feet with firing occurring at T of about 1.5 seconds. The terms J and D/F in the elevation signal are corrections to account for rocket ballistics. A voltage proportional to the true range R is used in equation (3); however, in equations (1) and (2) the range R is a servo shaft output which is limited to 5000 yards. In the computation of T the quantities R, $\dot{R}$, and $F \cos A_a \cos E_a$ are filtered as shown in figure 3. Additional time lags which are inherent in the mechanization of equations (1) to (3) have been considered negligible.

The attack is divided into three phases. During phase I, T is at its limit value of 20 seconds. Phase II begins as T becomes less than 20 seconds and, finally, in phase III, the azimuth steering signal is set to zero and no further corrections in azimuth are called for. Instead, T and F are varied to compensate for any azimuth steering error that may exist. The phase III relay engages at $T = 4.5$ seconds provided that $\dot{R}$ is greater than 75 yards per second and $|A_a|$ is greater than 19°, otherwise the system remains in phase II. The supplementary calculations for phase III are omitted because they are not pertinent to this report.

Automatic Attack Coupler

A detailed description of the networks used to convert the steering signals S_k and S_j into appropriate autopilot commands is given in reference 2. The block diagram of figure 4 illustrates the functions of the control surface tie-in, which are briefly summarized in the following paragraphs.

The steering signals S_k and S_j are converted to acceleration commands A_k and A_j by the proportionality factor K_1. The desired normal acceleration is then expressed as

$$A_{L_D} = QA_k + \cos \varphi$$

and the roll command to the aileron servo as

$$\varphi_\epsilon = \frac{QA'_j - \sin \varphi - K_p p}{|QA_k| + 1}$$

[redacted]

The gain K_1 is a function of altitude and is increased by a factor of approximately 1.7 upon entering phase II of the attack.

When A_{L_D} exceeds a preset maximum allowable value, the gain Q in a pair of variable gain amplifiers is automatically reduced until A_{L_D} is within the desired limits. Thus when A_{L_D} is less than its limit value Q is 1.0, but when A_{L_D} exceeds the limit, Q is effectively equal to

$$\frac{A_{L_{D(max)}} - \cos \varphi}{A_k}$$

The same gain reduction takes place in the azimuth channel to preserve the coordination between bank angle and normal acceleration.

The quantity A_{L_D} is compared to the measured normal acceleration and commands an elevator deflection proportional to error. The large time constant (6.8 sec) makes possible high steady-state gain while an acceptable margin of stability is still retained. The gain K_e is a a function of Mach number and altitude.

The primary stabilizing feedback in the azimuth channel is $\sin \varphi$; however, a roll-rate feedback ($K_p p$) is used to provide additional damping.

A 1-second filter also is included in the azimuth channel to minimize the effects of radar noise. The feedback $A_k p$ is used in conjunction with this filter as a cross roll correction to reduce steering signal lags which would normally accompany interceptor rolling motions.

Airplane-Autopilot Combination

The automatic control system utilizes the standard F-86D elevator and aileron servos so that only the inputs to the basic autopilot are modified. The yaw damper functions in its normal manner independently of the rest of the system.

FLIGHT INSTRUMENTATION

Data taken during the flights were recorded on a pair of 18 channel oscillographs. One contained the pertinent records from the radar and computer; these quantities consisted of R, $\dot{R}$, T, A_a, E_a, ω_j', ω_k', S_k, and S_j. On the second oscillograph were recorded the interceptor accelerations, angular velocities, angular attitudes, and control surface positions. In addition, static and dynamic pressure for computing

[redacted]

airspeed and altitude were recorded on a separate instrument. All flight records were synchronized at 0.1-second intervals by a common timing circuit. Also included in the instrumentation was a 35-mm movie camera mounted ahead of the cockpit. This camera was aligned with the reference axis of the airplane and set to operate during the final 4.5 seconds of the attack. The purpose of the camera was to aid in assessing miss distances.

FLIGHT TEST PROCEDURES

Flights to date have consisted primarily of beam attacks against an F-84F target airplane. These were made at altitudes of 20,000 and 30,000 feet in the Mach number range of 0.7 to 0.85. In most cases, a 1:1 target-interceptor speed ratio was used, and the attacks were initiated from a pattern which would result in a 90° beam attack with an initial azimuth antenna angle of approximately 45°.

The use of the F-84F as a target was dictated primarily by its availability, but because of poor radar reflection characteristics, radar lock-on generally could not be made at more than five miles range. The addition of corner reflectors in underwing tanks, however, increased the effective lock-on range to about 15 miles.

To study the effects of initial steering errors in azimuth and elevation, the interceptor was steered off the correct beam attack course before the automatic control system was engaged.

ANALOG-COMPUTER SIMULATION

A simulation of the complete lead-collision attack was carried out on the Ames analog computer. Each of the physical components of the system as well as the space geometry was represented so that the attack could be simulated from lock-on until firing. The scope and limitations of the analog representation are defined in the following paragraphs:

1. The radar and attack computer were represented as shown in figure 3; servo time lags and rocket ballistics terms were neglected. Also included was the switching through phases I, II, and III.

2. The simulation of the attack coupler included all the functions shown in figure 4.

3. The elevator servo was represented as a linear second-order system and the aileron servo as a simple first-order time expression. The combined yaw-damper and rudder servo response was defined by an equation of the form

[redacted]

$$\frac{\delta_r}{r} = \frac{Ks}{1 + \tau s}$$

4. The interceptor was represented as a five-degree-of-freedom system and was assumed to fly at constant velocity. Inertia cross-coupling terms were included, but all aerodynamic derivatives were assumed to be linear. The airplane equations of motion are given in Appendix B.

5. The target was assumed to fly a straight course at constant speed.

6. The relations used to convert relative interceptor-target motions into the equivalent range and line-of-sight information sensed by the radar are developed in Appendix C. The major assumption in these geometric relations is that small-angle approximations can be used to define the pitch attitude of the interceptor.

Except for a restriction on initial range (5 miles), simulated attacks could be initiated with unlimited freedom in both the location and heading of the interceptor with respect to the target. By a change of the voltage scales on the computer this restriction on range could be varied.

For this report simulated attacks were started from a precomputed initial position which would result in a geometrically perfect 90° beam lead-collision course as shown in sketch (a).

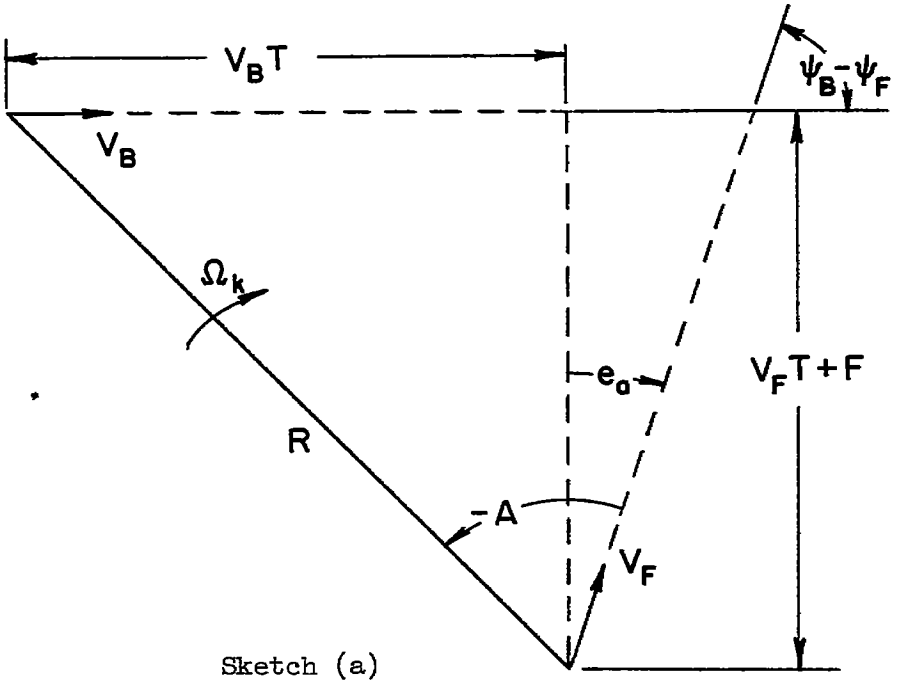

Sketch (a)

[redacted]

The initial heading of the interceptor was then varied to give steering errors in either azimuth or elevation. For the specified initial position, the steering error e_a is considered to be positive if the heading of the interceptor relative to the target is less than 90°.

RESULTS AND DISCUSSION

The following paragraphs present flight and analog-computer results which illustrate the effects of imperfect antenna space stabilization on the performance of the over-all system. Also presented is a stability analysis and a means for artificially alleviating the undesirable antenna response to interceptor motions.

Comparison of Flight and Simulated Results

When the response of the interceptor to azimuth steering errors was examined on the analog computer, two distinct phenomena were observed. First when the steering error was negative[1] the response was characterized by a pitch-down and a violent rolling motion. An example of this type of maneuver is shown by the solid lines of figure 5. Plotted here as functions of time from lock-on until firing are the range, time to go, the steering signals, the antenna angles, and the airplane responses in roll and normal acceleration. In this case the initial steering error was -10°; however, similar time histories were obtained for errors ranging from -5° to -30°. It was noted that this type of instability tended to accompany any maneuver in which the angle E_a became negative.

The same characteristics were later observed in flight as shown in figure 6. Here the interceptor started an attack on an approximate 90° beam collision course but with an initial azimuth steering error of about -10°. The quantities plotted are the same as in figure 5, and it will be noted that the character of the response is very similar although no attempt was made to duplicate precisely the initial conditions used on the computer. Furthermore, the flight records contain radar noise and saturation effects that were not included in the analog simulation and, as a result, the effects observed in flight were generally less severe.

The second phenomenon observed on the computer is illustrated in figure 7 as a very distinct unstable oscillation of the radar. Here the attack was initiated with a +20° azimuth steering error which required the interceptor to roll toward the target, thus creating a positive

[1]With a negative steering error (as defined in sketch (a)) the interceptor is commanded to roll away from the target, thus causing the antenna elevation angle to become negative.

antenna elevation angle. It will be noted that, in spite of the unstable steering signals for $K_2 = 31$, the roll response is reasonably smooth; however, there is an oscillation and a definite lag in the build-up of normal acceleration. This type of instability was generally encountered whenever the angle E_a exceeded a critical value of about 40°.

Figure 8 illustrates a flight attack in which a similar type of radar instability was observed. Because of radar noise the oscillations in the steering signals are not so well defined as in figure 7; however, a large build-up in S_j occurs as E_a becomes positive. For example S_j reaches a peak value of ±250 yards per second while from the geometry of the attack a true steering signal of about -50 yards per second should be expected.

Effect of Varying Stabilization Loop Gain

It was noted on the computer that the deficiencies described in the previous paragraphs could be eliminated almost entirely by increasing the antenna space-stabilization loop gain K_2 in both channels of the radar. The dotted lines on figures 5 and 7 show the improvement obtained by increasing K_2 from its nominal value of 31 to 62. Also shown by the dash-dot line is the further improvement that could be obtained with an infinitely large K_2.

The closed-loop transfer function for the complete azimuth channel including both line of sight (Ω_K) and airplane rate (W_k) inputs is (from fig. 3)

$$\omega_k' = \frac{G_1(s + G_2 \cos E_a)\Omega_K - G_1 s W_k}{s^2 + (G_2 \cos E_a)s + G_1 G_2 \cos E_a} \tag{4}$$

In this expression for ω_k' it is assumed that $W_k = W_K$ and that $E = E_a$ (see Appendix C). The transfer function for the elevation channel is of the same form except that there are no cosine terms.

Equation (4) and the analogous equation for the elevation channel are each of the form

$$\omega' = f(\Omega) + f(W)$$

The function $f(\Omega)$ represents true steering information from the angular rate of the line of sight while $f(W)$ is an erroneous signal due to the angular velocity of the interceptor. During a maneuver in which there is a large rolling velocity, $f(W)$ may reach a magnitude equal to or even greater than $f(\Omega)$ and be of the same or opposite sign. For the case

[redacted]

illustrated in figure 5, for example, $f(\Omega_K)$ and $f(W_k)$ are both positive during the first 2 seconds, thus leading to an excessively large value of the azimuth steering signal S_j and an overshoot in roll. During the same period of time $f(\Omega_J)$ becomes positive and $f(W_j)$ reaches a large enough negative value to cause a negative S_k and an initial pitch-down motion. These effects vanish as the gain K_2 is increased. In either channel when K_2 becomes infinitely large equation (4) reduces to

$$\omega_k' = \frac{G_1\Omega_K}{s + G_1} \tag{5}$$

Unfortunately in the actual interceptor system it is not practical to increase the gain K_2 in this manner. Any appreciable increase above the nominal range of 30 to 35 results in an intolerable high-frequency oscillation or "jitter" of the antenna. This characteristic was not detected on the analog computer because the antenna drive G_2 was represented as a linear first-order term; however, the actual drive system is of higher order and contains nonlinearities such as friction and backlash.

When the expressions for G_1 and G_2 given in figure 3 are substituted into the characteristic equation and when an instantaneous constant value is assumed for E_a, the radar system is found to be stable for all values of $K_2\cos E_a$ greater than 2.0. For values lower than 2.0 there is a low-frequency oscillatory instability. When the characteristic equation is examined with a second-order representation for G_2, the same low-frequency instability appears and, in addition, for large values of $K_2\cos E_a$, the system exhibits the high-frequency jitter that was noted in the actual radar. In this case, the upper limit on K_2 depends on the definition of G_2.

Stability Analysis of Radar With Airplane Rate Feedback

As shown in the previous sections, the radar during an attack can become unstable and the degree as well as the type of instability depends primarily on the antenna stabilization loop gain and the instantaneous elevation angle E_a. Furthermore, when the radar loop alone is examined under the same conditions, it is found to be stable. This suggested that the feedback due to interceptor motions was destabilizing.

For the cases illustrated in figures 5 to 8 the airplane maneuvers first in roll, and since q and r initially are small compared to p, the airplane rate input to the azimuth channel can be approximated as

$$W_k = p \cos A_a \sin E_a$$

[redacted]

By the use of this expression for W_k it is possible to examine the radar with the additional airplane rate feedback as illustrated in the block diagram of figure 9. The term G_3 is the over-all transfer function of the attack computer, coupler, aileron servo, and the airplane. Then K_3 is the corresponding total gain (i.e., roll rate of the airplane per unit antenna rate). The term $R\omega_k'$ in the attack computer is considered large as compared to $(F \sin A)/T$, and thus the gain K_3 is a direct function of range.

The transfer function for this complete loop is

$$\frac{\omega_k'}{\Omega_K} = \frac{G_1(s + G_2 \cos E_a)}{s^2 + (G_2 \cos E_a + G_1 G_3 \cos A_a \sin E_a)s + G_1 G_2 \cos E_a} \tag{6}$$

Again it is assumed that $W_k = W_K$ and that $E_a = E$. It should also be noted that $\cos E_a$ appears only with G_2 and $\sin E_a$ with G_3.

Examination of the characteristic equation with instantaneous values of A_a and E_a shows the combined radar-airplane rate loop to be conditionally stable. Analysis of this loop with a simple representation for G_3 indicated the stability to be primarily a function of the gains K_2 and K_3 and the angle E_a. (The second term in the characteristic equation changes sign when E_a reaches a relatively small negative value.) The results of this analysis are summarized in figure 10. The curves labeled $K_4 = 0$ are the stability boundaries plotted as functions of $K_3 \sin E_a$ and $K_2 \cos E_a$. For negative values of E_a the response is divergent and for positive E_a the response becomes oscillatory. Considering excursions of E_a through $\pm 60^\circ$ the dotted line indicates the normal operating range of the system with fixed gains, and thus it may enter either unstable region.

The information given in figure 10 should be considered only as qualitative. The exact shape and location of the boundaries depend to some extent on the simplifying assumptions made; however, by means of analog-computer as well as hand calculations the existence of the boundaries has definitely been established. Furthermore, when W_k was represented by a more exact expression which included r, the analog computer indicated little change in the location of the boundaries. It should also be pointed out that figure 10 does not include the high-frequency jitter usually encountered when $K_2 \cos E_a$ exceeds a value of approximately 45.

A similar loop exists in the elevation channel. Here the airplane rate feedback term W_j is

[redacted]

$$W_j = q \cos A_a - p \sin A_a$$

The transfer function ω_j'/Ω_J is thus independent of the angle E_a, and because of lower gain levels as well as the absence of sign changes, there does not appear to be a well-defined stability problem in this channel. Nevertheless, the airplane rate signal, as mentioned earlier, does provide erroneous steering signals in elevation.

A Method for Canceling the Effects of Airplane Rate Feedback

Since it is generally not practical to improve the stability of the combined radar-airplane rate response by increasing the system gains, it appeared that perhaps the effects of airplane motions could be canceled by using additional feedback signals in the radar loop. Several possible schemes were examined, and one which appeared promising is shown in the block diagram of figure 11. This consists of a feedback of gain K_4 from the output of the integrating rate gyro to the input of the receiver lead-lag networks.

With this feedback the transfer function of the radar alone (azimuth channel) becomes, in place of equation (4),

$$\omega_k' = \frac{G_1(s + G_2\cos E_a)\Omega_K - G_1 s(1 - K_4)W_k}{s^2 + (G_2\cos E_a + G_1K_4)s + G_1G_2\cos E_a} \tag{7}$$

Now, if $K_4 = 1$ this reduces to

$$\omega_k' = \frac{G_1(s + G_2\cos E_a)\Omega_K}{s^2 + (G_2\cos E_a + G_1)s + G_1G_2\cos E_a} = \frac{G_1\Omega_K}{s + G_1} \tag{8}$$

which is identical to equation (5), and thus the response of the antenna to interceptor motions is completely eliminated.

With the compensating feedback the transfer function of the complete radar-airplane loop becomes

$$\frac{\omega_K'}{\Omega_K} = \frac{G_1(s + G_2\cos E_a)}{s^2 + [G_2\cos E_a + G_1K_4 + G_1G_3\cos A(1 - K_4)\sin E_a]s + G_1G_2\cos E_a} \tag{9}$$

[redacted]

When $K_4 = 0$ this is the same as equation (6), but when $K_4 = 1$ it reduces to

$$\frac{\omega_k'}{\Omega_K} = \frac{G_1}{s + G_1}$$

which again is the same as equation (5). Thus with unity feedback the effects of interceptor motions are canceled, and dynamically the radar acts as if it were perfectly space stabilized.

If K_4 is less than 1.0 partial compensation can be expected; however, if K_4 is greater than 1.0 the system can again become unstable since the second term in the denominator of equation (9) can become negative for relatively small positive values of E_a. Since it would be physically difficult to set the feedback gain at precisely 1.0, calculations were made for a gain of 0.8, and the marked improvement in the stability boundaries is shown in figure 10 (theoretically for $K_4 = 1.0$ the system would be stable over the entire region).

When the complete attack problem was run on the analog computer, a substantial improvement was noted in the system response for values of K_4 from 0.4 to 0.9. The optimum value appeared to be about 0.8. There was a sharp deterioration in stability as a value of 1.0 was exceeded. Figure 12 illustrates the marked improvement obtainable with $K_4 = 0.8$ in both channels and it can be seen that the results compare favorably to those for a perfectly stabilized radar. Even though the stability problem was not directly apparent in the elevation channel, it was necessary to include the compensating feedback in this channel in order to isolate it from the effects of airplane rate feedback.

The feedback loop proposed here appeared to be the easiest to mechanize of various conceivable schemes for improving the response of a radar. It should be possible to achieve essentially the same effect by modifying the antenna rate signals ω_j' and ω_k' (or the steering signals, S_k and S_j) by appropriate functions of p. The use of compensating feedbacks would appear in many cases to be more desirable than the straightforward or "brute force" method of increasing stabilization loop gains by using greater power and higher precision components in the antenna drive. The proposed method enables adequate performance to be obtained with relatively low power and also makes the system less sensitive to inadvertent gain changes.

One drawback to the compensating feedback is that it effectively reduces the tracking loop gain; that is, for a given line-of-sight rate the antenna will track a target with a larger error angle ϵ.

For the basic system the steady-state tracking loop gain is

[redacted]

$$\left|\frac{\omega_k'}{\epsilon_A}\right|_{ss} = K_1$$

and for the modified system

$$\left|\frac{\omega_k'}{\epsilon_A}\right|_{ss} = \frac{K_1 K_2 \cos E_a}{K_1 K_4 + K_2 \cos E_a}$$

In figure 13 the steady-state gain is plotted as a function of $K_2 \cos E_a$ (the effective stabilization loop gain) for two values of K_4. For $K_2 \cos E_a$ of 31 and K_4 of 0.8 the tracking loop gain is 18.5 as compared to 35.2 for the unmodified system. The resulting increase in tracking error, however, does not appear to be too significant.

Because the problems of imperfect space stabilization are directly related to airplane roll response, it is desirable to design the roll control system to prevent excessive roll rates and bank-angle overshoots. With an optimum type of roll control such as discussed in reference 3 stabilization loop effects can be decreased to some extent. Furthermore, for gun-firing interceptors the roll stability can be further improved, as indicated in reference 4, by a positive inclination of the gun line with respect to the interceptor roll axis.

CONCLUSIONS

A flight and analog-computer investigation has been conducted to examine the effects of tracking radar dynamics on the response of an automatic interceptor system. The results show that imperfect space stabilization of the radar antenna can lead to serious deficiencies in system performance. The fact that the antenna responds to airplane motions as well as line-of-sight rates leads to erroneous steering signals and, under certain conditions, to an unstable over-all system response.

In the present study various schemes for canceling the airplane rate inputs to the radar were investigated. One such scheme completely eliminated the tendency toward instability over the normal range of operating conditions and gave a system response comparable to that obtainable with a perfectly stabilized radar. The use of such a device enables fast response with a relatively low-powered antenna drive and, furthermore, makes the system less sensitive to gain adjustments.

Ames Aeronautical Laboratory
National Advisory Committee for Aeronautics
Moffett Field, Calif., Nov. 19, 1956

[redacted]

APPENDIX A

DEFINITION OF COORDINATE SYSTEMS

The axis systems used in this report are defined in the following paragraphs. Each is a right-hand Cartesian coordinate system. Rotations are considered positive if they are in a clockwise sense when viewed in the positive direction of the axis of rotation.

Interceptor Body Axis System (x,y,z)

The x axis of this system is the fuselage reference line; the y axis is perpendicular to the plane of symmetry; and the z axis is perpendicular to both the x and y axes. This axis system is oriented with respect to earth by the angles ψ, θ, and φ taken in that order; ψ is measured in the horizontal plane, and θ in the vertical plane to establish the direction of the x axis; φ is then measured normal to the x axis (in the yz plane).

Interceptor Wind Axis System (X,Y,Z)

The X axis is in the direction of the interceptor velocity vector, and the Y axis lies in the xy plane perpendicular to the X axis; the space orientation angles of this axis system are designated by ψ_F, θ_F, and φ_F.

As shown in sketch (b) the relative orientation of the body and wind axis systems is defined by the angles $-\beta$ and α. The angle β is measured in the XY plane and α in the plane of symmetry of the interceptor.

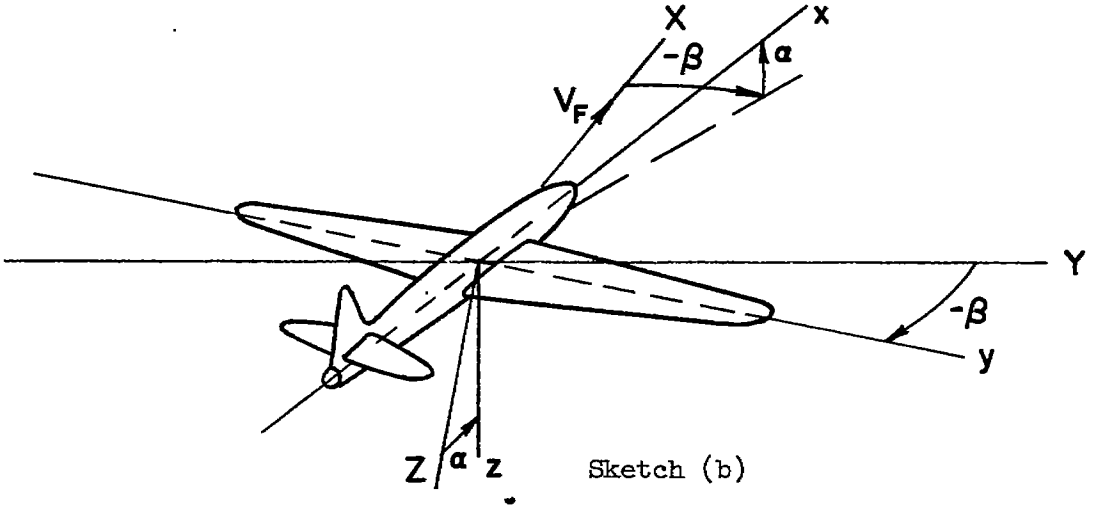

Sketch (b)

[redacted]

Line-of-Sight Coordinate System (I,J,K)

The I,J,K coordinate system has its I axis along the line of sight and the J axis in the xy plane. The orientation of this system with respect to the x,y,z axes is defined by the angles A and E as shown in sketch (c).

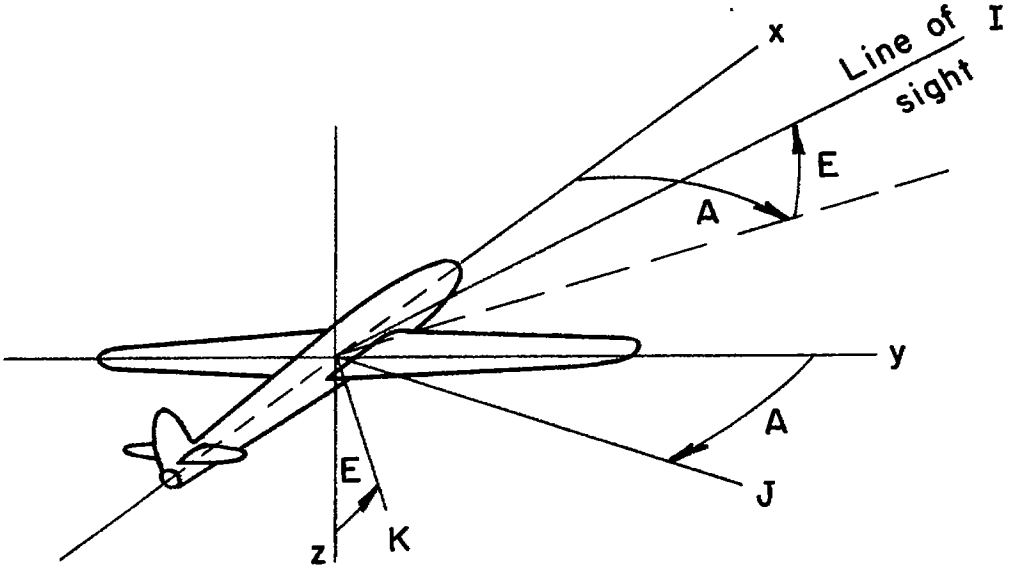

Sketch (c)

Antenna Coordinate System (i,j,k)

The i axis of this system is in the direction of the antenna (tracking line), and j is in the xy plane of the interceptor. This system is oriented with respect to the interceptor body axes by the angles A_a and E_a.

The following chart summarizes the orientation of the various axis systems:

Orientation of - / With respect to -	Body axes, xyz	Wind axes, XYZ	Line-of-sight axes, IJK	Antenna axes, ijk
Earth	ψ,θ,φ	$\psi_F,\theta_F,\varphi_F$	---	---
xyz	---	---	A,E	A_a,E_a
XYZ	$-\beta,\alpha$	---	---	---

[redacted]

APPENDIX B

AIRPLANE EQUATIONS OF MOTION

In the simulation of the attack problem on the analog computer the following equations were used to describe the motions of the interceptor. It was assumed that the interceptor flies at constant velocity and that small-angle approximations can be used to define its pitch attitude.

$$\dot{p} + A_1qr - A_2(\dot{r} + pq) - L_pp - L_rr - L_\beta\beta - L_{\delta_a}\delta_a - L_{\delta_r}\delta_r = 0$$

$$\dot{q} + A_3rp - A_4(r^2 - p^2) - M_\alpha\alpha - M_{\dot{\alpha}}\dot{\alpha} - M_qq - M_{\delta_H}\delta_H = 0$$

$$\dot{r} + A_5pq - A_6(\dot{p} - qr) - N_pp - N_rr - N_\beta\beta - N_{\delta_a}\delta_a - N_{\delta_r}\delta_r = 0$$

$$\dot{\beta} + r - p\alpha - \frac{g}{V_F}\sin\varphi_F - Y_\beta\beta - Y_{\delta_r}\delta_r = 0$$

$$\dot{\alpha} - q + p\beta - \frac{g}{V_F}\cos\varphi_F - Z_\alpha\alpha - Z_{\delta_H}\delta_H = 0$$

where

$$A_1 = \frac{I_z - I_y}{I_x}, \qquad A_2 = \frac{I_{xz}}{I_x}$$

$$A_3 = \frac{I_x - I_z}{I_y}, \qquad A_4 = \frac{I_{xz}}{I_y}$$

$$A_5 = \frac{I_y - I_x}{I_z}, \qquad A_6 = \frac{I_{xz}}{I_z}$$

and the aerodynamic force and moment parameters are defined as

[redacted]

$$L_p = B_x \frac{b}{2V_F} \frac{dC_l}{d(pb/2V_F)} \qquad N_p = B_z \frac{b}{2V_F} \frac{dC_n}{d(pb/2V_F)}$$

$$L_r = B_x \frac{b}{2V_F} \frac{dC_l}{d(rb/2V_F)} \qquad N_r = B_z \frac{b}{2V_F} \frac{dC_n}{d(rb/2V_F)}$$

$$L_\beta = B_x \frac{dC_l}{d\beta} \qquad N_\beta = B_z \frac{dC_n}{d\beta}$$

$$L_\delta = B_x \frac{dC_l}{d\delta} \qquad N_\delta = B_z \frac{dC_n}{d\delta}$$

$$M_\alpha = B_y \frac{dC_m}{d\alpha} \qquad Z_\alpha = -\frac{q_\infty S}{mV_F} \frac{dC_L}{d\alpha}$$

$$M_{\dot{\alpha}} = B_y \frac{\bar{c}}{2V_F} \frac{dC_m}{d(\dot{\alpha}\bar{c}/2V_F)} \qquad Z_\delta = -\frac{q_\infty S}{mV_F} \frac{dC_L}{d\delta}$$

$$M_q = B_y \frac{\bar{c}}{2V_F} \frac{dC_m}{d(q\bar{c}/2V_F)} \qquad Y_\beta = \frac{q_\infty S}{mV_F} \frac{dC_Y}{d\beta}$$

$$M_\delta = B_y \frac{dC_m}{d\delta}$$

where

$$B_x = \frac{q_\infty Sb}{I_x}$$

$$B_y = \frac{q_\infty S\bar{c}}{I_y}$$

$$B_z = \frac{q_\infty Sb}{I_z}$$

The terms qr and r^2 appeared to be of negligible importance and were subsequently omitted from the simulation.

[redacted]

APPENDIX C

DEVELOPMENT OF THE SPACE GEOMETRY OF THE LEAD-COLLISION ATTACK

In order to simulate the lead-collision attack on an analog computer, it is necessary to describe completely the space geometry involved. The method used in the present investigation involves the following steps:

1. Project the target velocity vector into interceptor wind axis coordinates.

2. Determine the three components of relative velocity.

3. Resolve the relative velocity components into the line-of-sight coordinate system to obtain range rate and angular rates of the line of sight.

4. Resolve the interceptor angular rates into the line-of-sight coordinate system to obtain the orientation of the line of sight with respect to the interceptor. These steps are outlined in detail in the following paragraphs.

If p, q, and r are the angular velocities of the interceptor about its body axes, then the angular velocities about the wind axes (X,Y,Z) are:

$$\left.\begin{aligned} W_X &= (q - \dot{\alpha})\sin\beta + (p\cos\alpha + r\sin\alpha)\cos\beta \\ W_Y &= (q - \dot{\alpha})\cos\beta - (p\cos\alpha + r\sin\alpha)\sin\beta \\ W_Z &= r\cos\alpha - p\sin\alpha + \dot{\beta} \end{aligned}\right\} \qquad (C1)$$

If α and β are assumed to be small, the angular velocities become

$$\left.\begin{aligned} W_X &= p + r\alpha + (q - \dot{\alpha})\beta \\ W_Y &= q - \dot{\alpha} - p\beta \\ W_Z &= r + \dot{\beta} - p\alpha \end{aligned}\right\} \qquad (C2)$$

The space orientation of this wind axis system is defined by the Euler angles ψ_F, θ_F, and ϕ_F which may be determined from the following relations:

[redacted]

$$\left.\begin{aligned} \dot{\theta}_F &= W_Y \cos \varphi_F - W_Z \sin \varphi_F \\ \dot{\psi}_F \cos \theta_F &= W_Y \sin \varphi_F + W_Z \cos \varphi_F \\ \dot{\varphi}_F &= W_X + \dot{\psi}_F \sin \theta_F \end{aligned}\right\} \tag{C3}$$

If θ_F is restricted to small angles, these equations become (neglecting $(q - \dot{\alpha})\beta$)

$$\left.\begin{aligned} \dot{\theta}_F &= W_Y \cos \varphi_F - W_Z \sin \varphi_F \\ \dot{\psi}_F &= W_Y \sin \varphi_F + W_Z \cos \varphi_F \\ \dot{\varphi}_F &= p + r\alpha + \dot{\psi}_F \theta_F \end{aligned}\right\} \tag{C4}$$

If the target velocity V_B is oriented in space by the horizontal and vertical angles ψ_B and θ_B, then the components of its velocity in the interceptor wind axis system are given by

$$\left.\begin{aligned} V_{B_X} &= b \cos \theta_F + c \sin \theta_F \\ V_{B_Y} &= a \cos \varphi_F - (c \cos \theta_F - b \sin \theta_F) \sin \varphi_F \\ V_{B_Z} &= -(c \cos \theta_F - b \sin \theta_F) \cos \varphi_F - a \sin \varphi_F \end{aligned}\right\} \tag{C5}$$

where

$$a = V_B \cos \theta_B \sin(\psi_B - \psi_F)$$

$$b = V_B \cos \theta_B \cos(\psi_B - \psi_F)$$

$$c = V_B \sin \theta_B$$

It should be noted that there are no restrictions on the flight paths of either the target or the interceptor; however, in view of the assumptions made in the interceptor equations of motion it is necessary to restrict the angle θ_B to small values.

[redacted]

Since the interceptor velocity V_F lies along the X axis, the relative velocities in this coordinate system are

$$\left.\begin{aligned} V_X &= V_{B_X} - V_F \\ V_Y &= V_{B_Y} \\ V_Z &= V_{B_Z} \end{aligned}\right\} \tag{C6}$$

The relative velocities are then resolved into the interceptor body axis system (x,y,z) by the following relations:

$$\left.\begin{aligned} V_x &= (V_X\cos\beta - V_Y\sin\beta)\cos\alpha - V_Z\sin\alpha \\ V_y &= V_X\sin\beta + V_Y\cos\beta \\ V_z &= (V_X\cos\beta - V_Y\sin\beta)\sin\alpha + V_Z\cos\alpha \end{aligned}\right\} \tag{C7}$$

Again using small-angle approximations for α and β

$$\left.\begin{aligned} V_x &= V_X - V_Y\beta - V_Z\alpha \\ V_y &= V_Y + V_X\beta \\ V_z &= V_Z + V_X\alpha \end{aligned}\right\} \tag{C8}$$

The next step is to transform the relative velocities into the line-of-sight coordinate system (I,J,K) which has its I axis along the line of sight and its J axis in the xy plane of the interceptor. The two axes systems are oriented by the angles A and E. The following resolutions are required for this transformation:

$$\left.\begin{aligned} V_I &= (V_x\cos A + V_y\sin A)\cos E - V_z\sin E \\ V_J &= V_y\cos A - V_x\sin A \\ V_K &= (V_x\cos A + V_y\sin A)\sin E + V_z\cos E \end{aligned}\right\} \tag{C9}$$

By definition of the line-of-sight axis system, $V_I = \dot{R}$,

[redacted]

$$\Omega_J = -\frac{V_K}{R}$$

and

$$\Omega_K = \frac{V_J}{R}$$

To determine the orientation angles A and E it is necessary to know the angular rates of the interceptor expressed in the line-of-sight coordinate system. These are

$$\left.\begin{aligned} W_I &= (p \cos A + q \sin A)\cos E - r \sin E \\ W_J &= q \cos A - p \sin A \\ W_K &= (p \cos A + q \sin A)\sin E + r \cos E \end{aligned}\right\} \qquad (C10)$$

The relative rotation of the line of sight with respect to the interceptor may then be defined as

$$\dot{E} = \Omega_J - W_J$$

$$\dot{A} \cos E = \Omega_K - W_K$$

The quantities $\dot{E}$ and $\dot{A}$ serve as inputs to the elevation and azimuth channels of the radar, respectively. As shown in figure 3, these signals are compared to the antenna rates with respect to the interceptor ($\dot{E}_a$ and $\dot{A}_a$), and the difference is integrated to obtain the tracking error angles normally sensed by the radar. In the azimuth channel it is necessary to multiply by $\cos E_a$ in order to project the error angle from the body to the antenna axis system.

The integrating rate gyros in the radar are mounted on the antenna and thus sense the angular rates of the antenna in the antenna coordinate system (i,j,k) rather than in the line-of-sight system (I,J,K). These rates are then defined as

$$\omega_j = \dot{E}_a + W_j$$

$$\omega_k = \dot{A} \cos E_a + W_k$$

[redacted]

The angular velocities W_j and W_k can be obtained directly from p, q, and r by equations (C10) in which E and A are replaced by E_a and A_a, or more simply, ϵ_E and ϵ_A may be considered as the orientation of the line of sight with respect to the antenna and, thus,

$$W_j = W_J \cos \epsilon_A - W_I \sin \epsilon_A$$

$$W_k = (W_I \cos \epsilon_A + W_J \sin \epsilon_A) \sin \epsilon_E + W_K \cos \epsilon_E$$

and since ϵ_E and ϵ_A are very small angles

$$W_j \approx W_J - W_I \epsilon_A$$

$$W_k \approx W_K + W_I \epsilon_E$$

In the present investigation, however, the effects of these resolutions were considered to be negligible and it was assumed that $W_j = W_J$ and $W_k = W_K$.

[redacted]

REFERENCES

1. McVey, Bruce D.: An Electronic Rocket-Fire Control Computer, Type AN/APA 84. Hughes Aircraft Co. Tech. Memo. No. 314, July 1, 1953.

2. Anon.: Final Report Phase I Development of a Control Surface Tie-In Subsystem for the E-3/F-86D Weapon System. Res. and Dev. Labs., Hughes Aircraft Co., 28 Aug. 1953.

3. Triplett, William C.: Considerations Involved in the Design of a Roll-Angle Computer for a Bank-to-Turn Interceptor. NACA RM A55D18a, 1955.

4. Turner, Howard L., Triplett, William C., and White, John S.: A Flight and Analog Computer Study of Some Stabilization and Command Networks for an Automatically Controlled Interceptor During the Final Attack Phase. NACA RM A54J14, 1955.

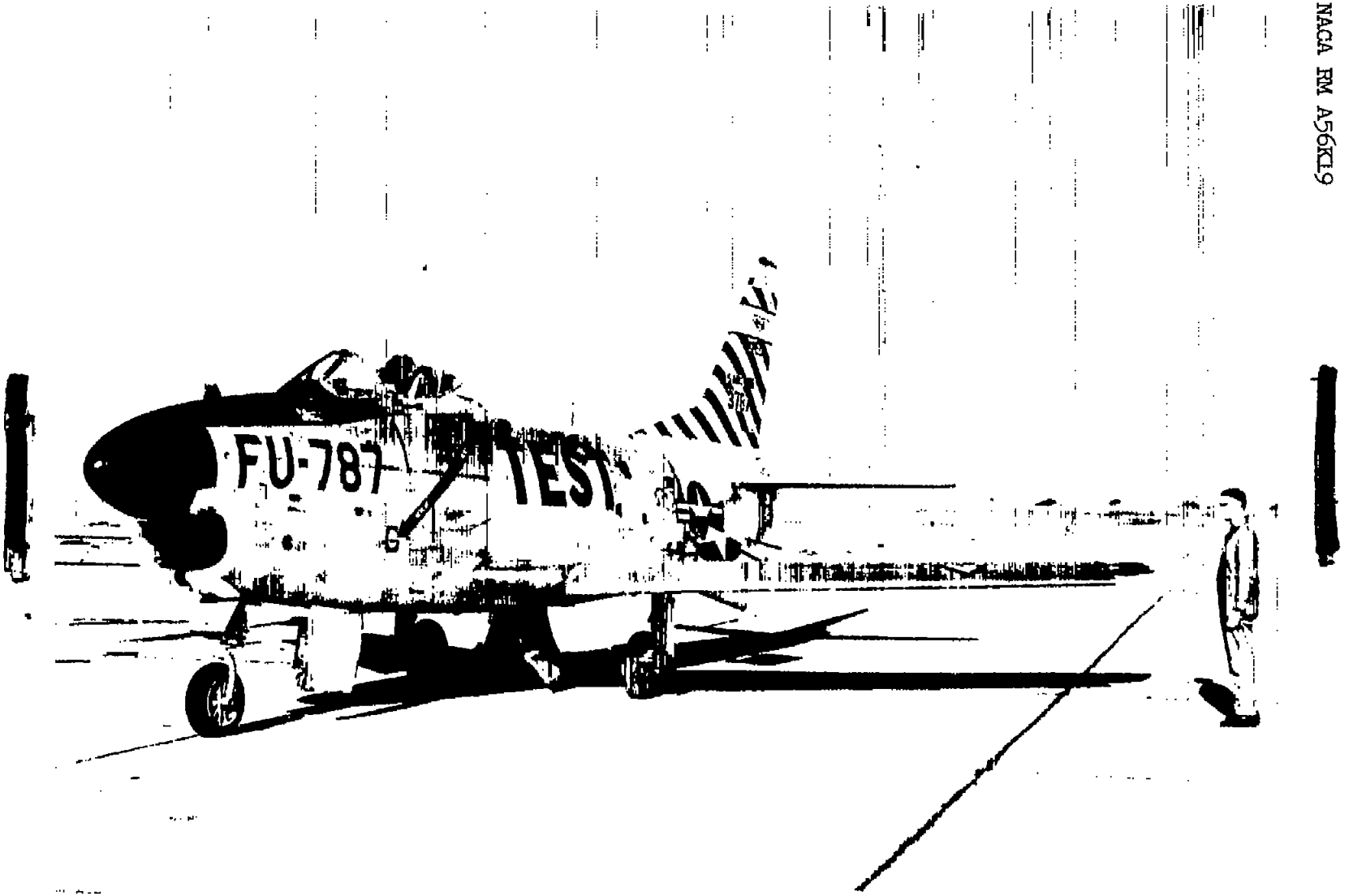

Figure 1.- Photograph of test airplane.

A-21022

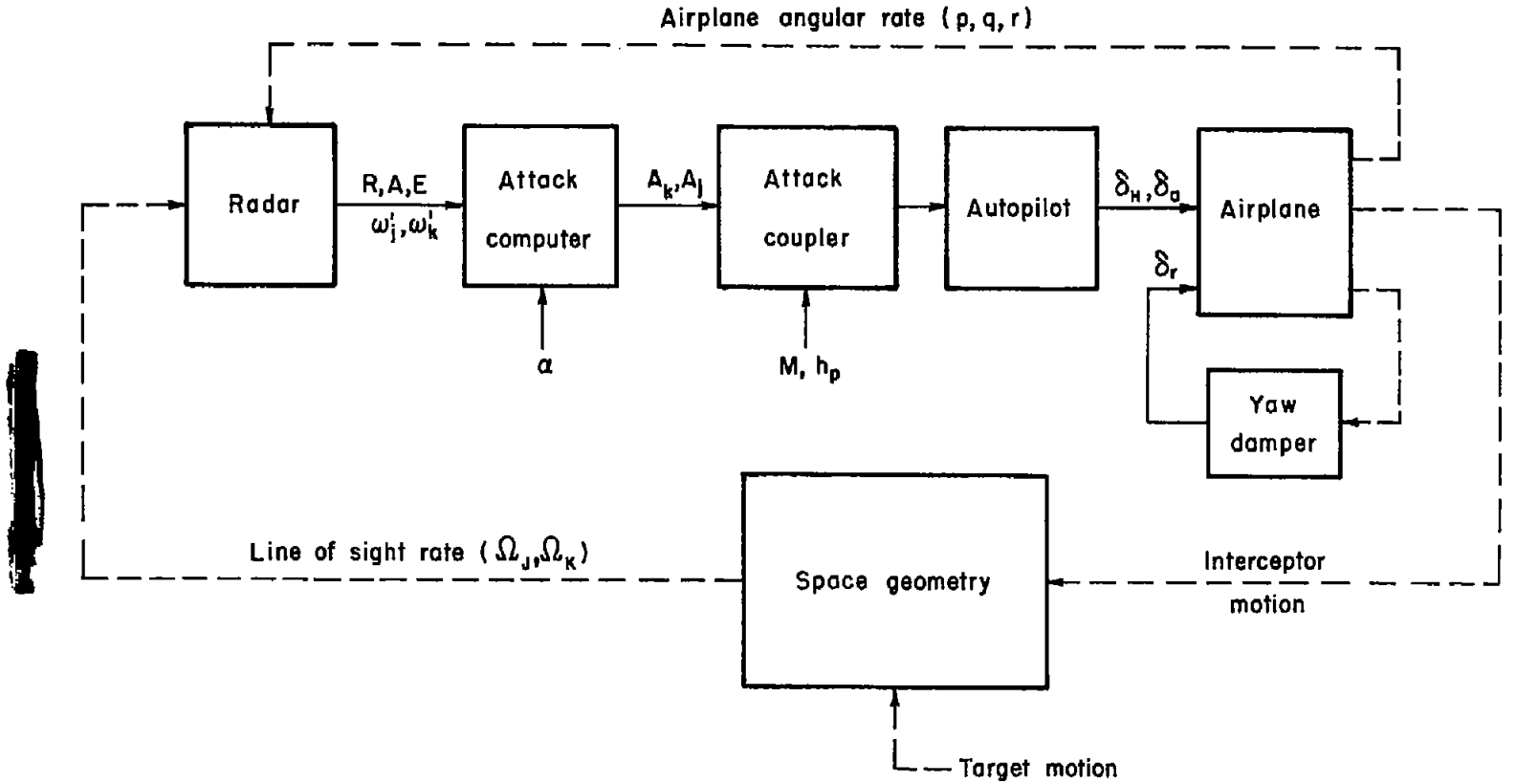

Figure 2.- Simplified diagram of automatic interceptor system.

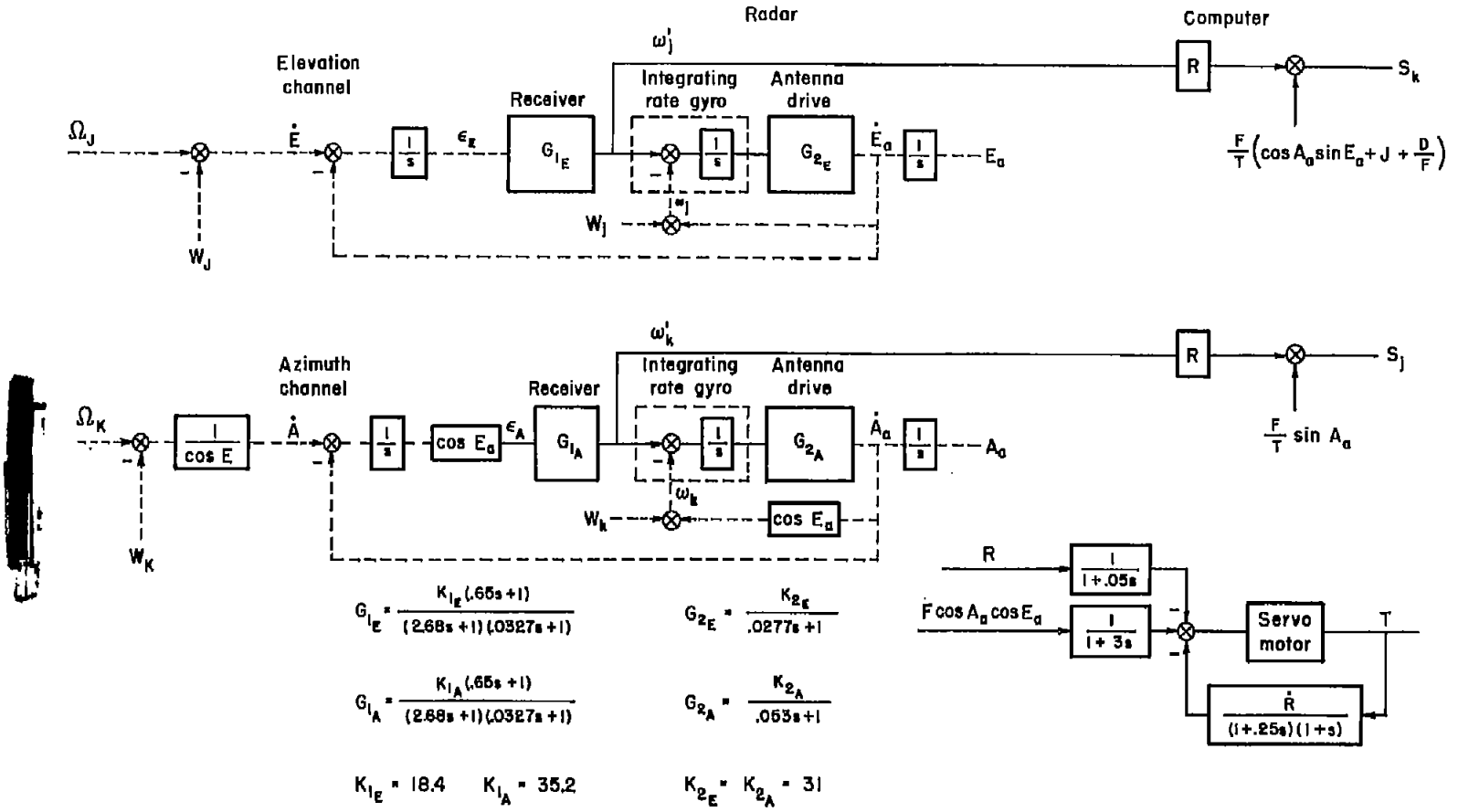

Figure 3.- Block diagram of radar and attack computer.

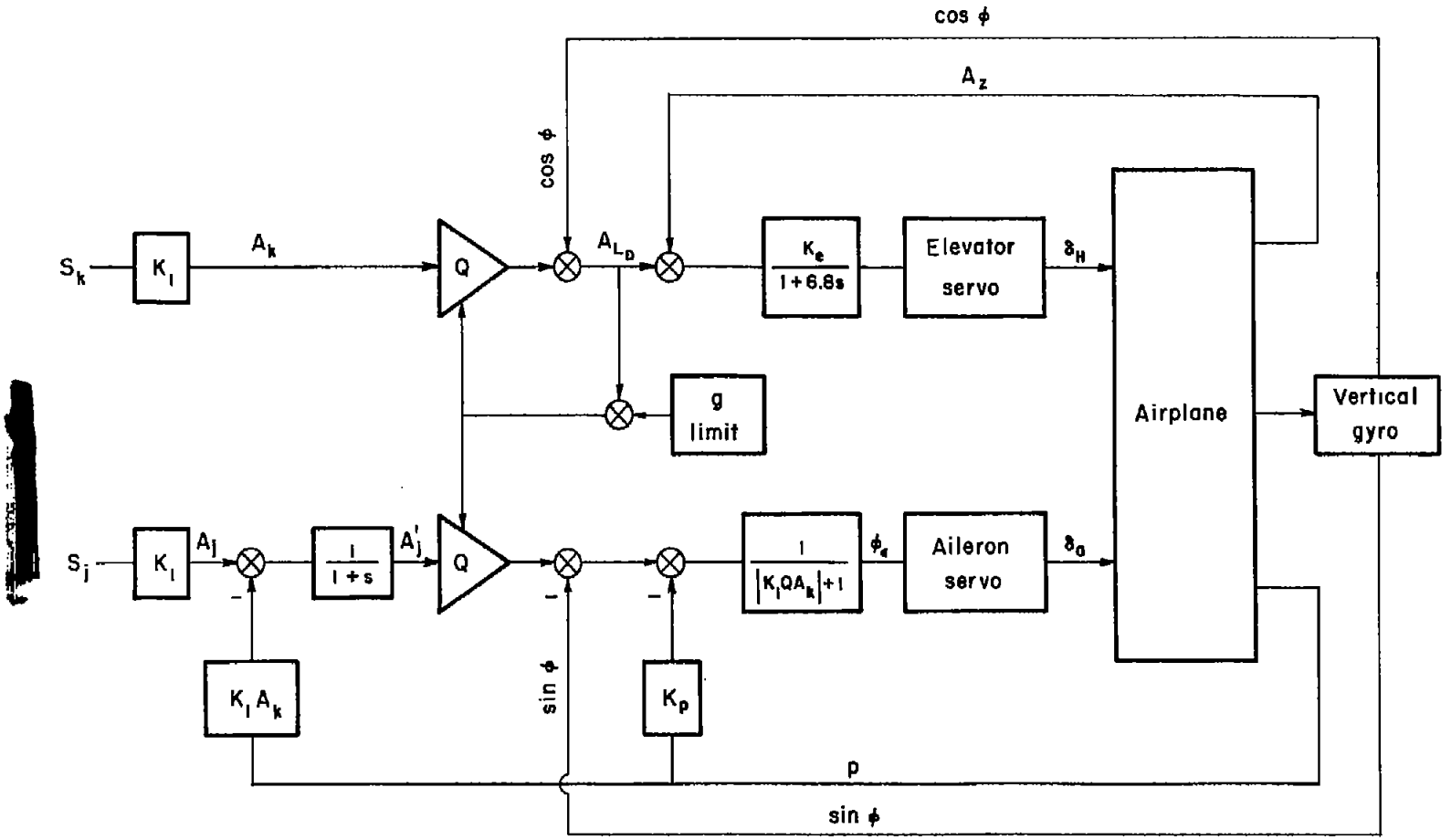

Figure 4.- Block diagram of automatic attack coupler.

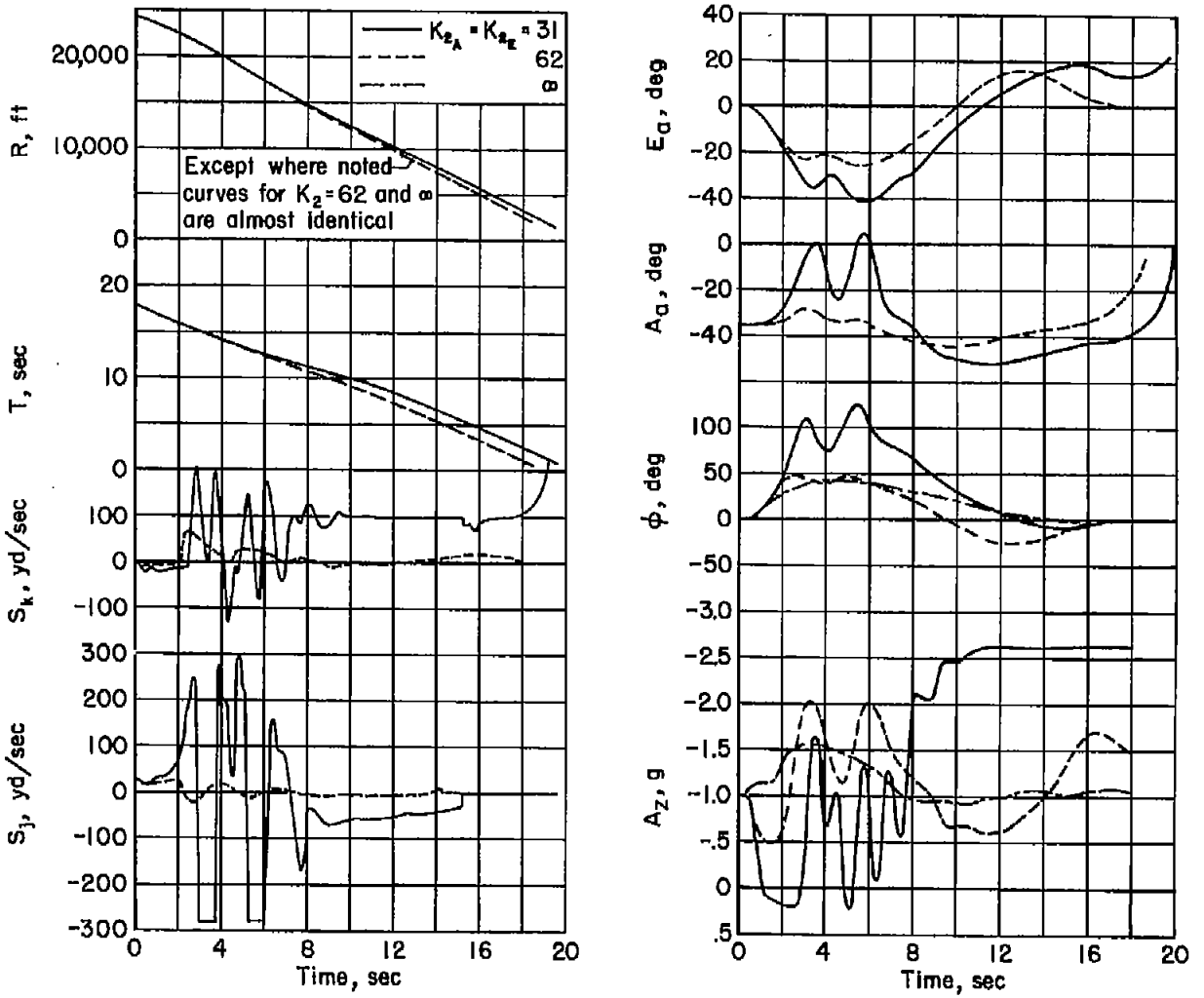

Figure 5.- Analog-computer time history of beam attack (-10° initial azimuth steering error) for three values of antenna stabilization loop gain.

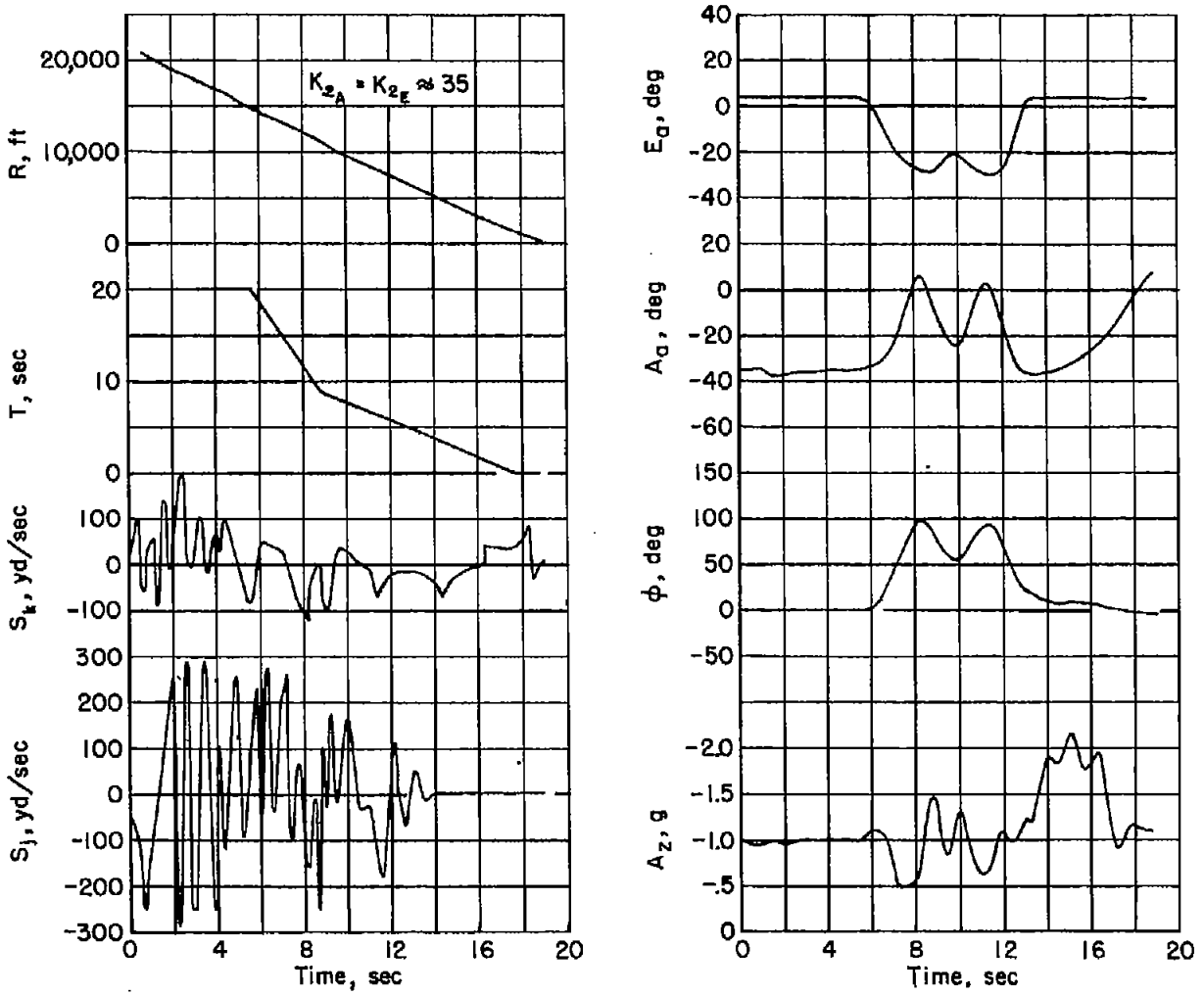

Figure 6.- Typical flight time history of beam attack (-10° initial azimuth steering error).

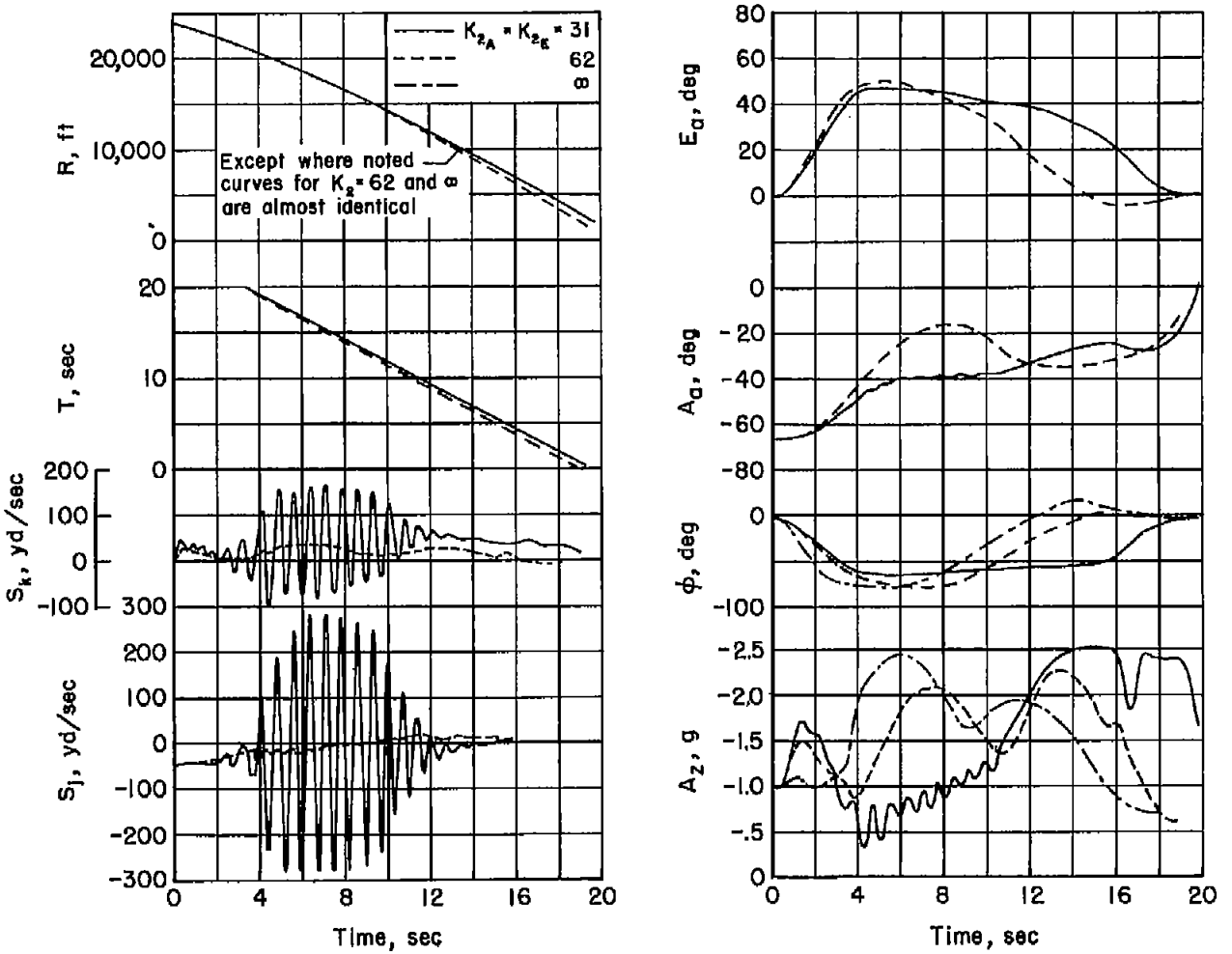

Figure 7.- Analog-computer time history of beam attack (20° initial azimuth steering error) for three values of antenna stabilization loop gain.

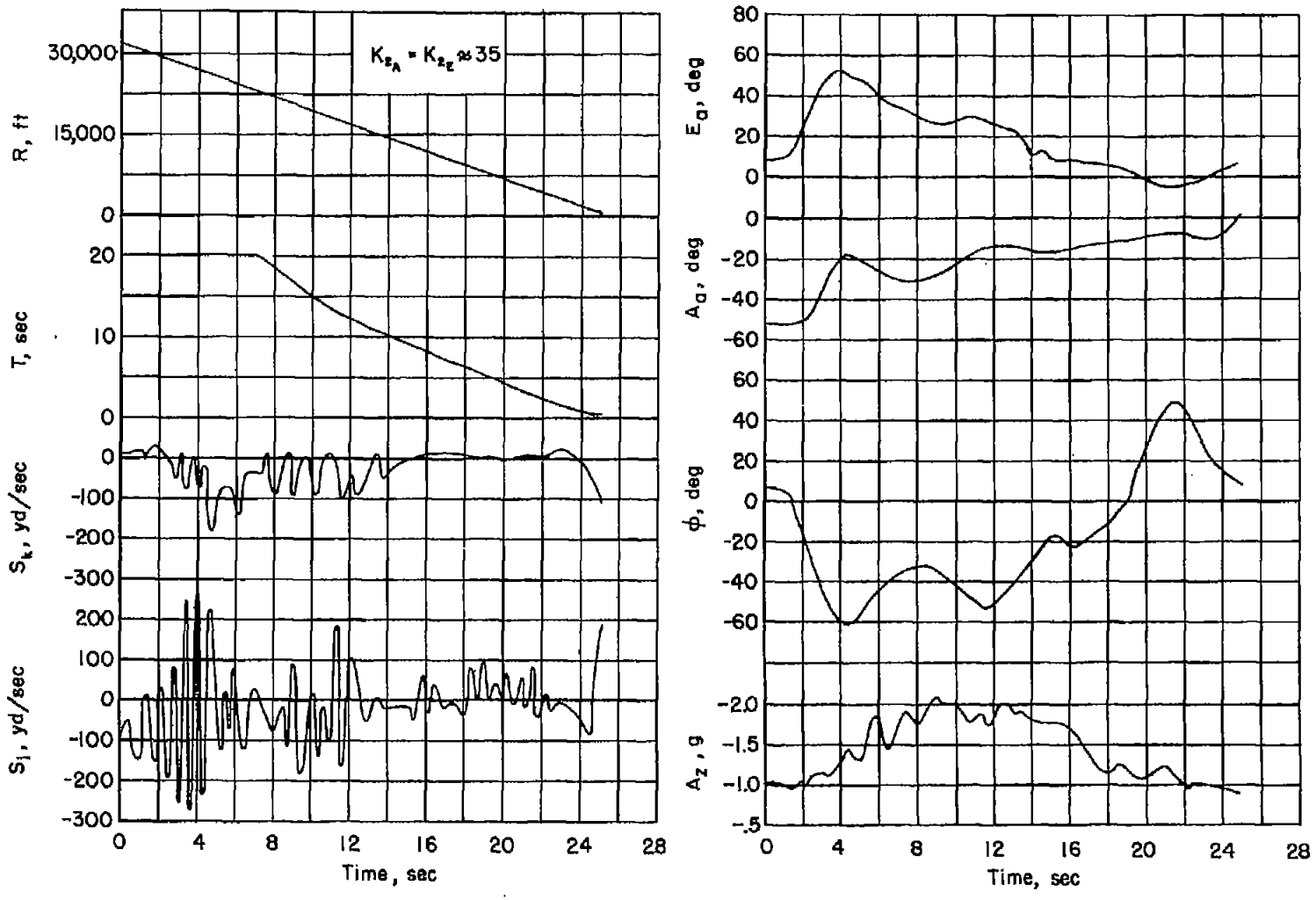

Figure 8.- Typical flight time history of beam attack (positive azimuth steering error).

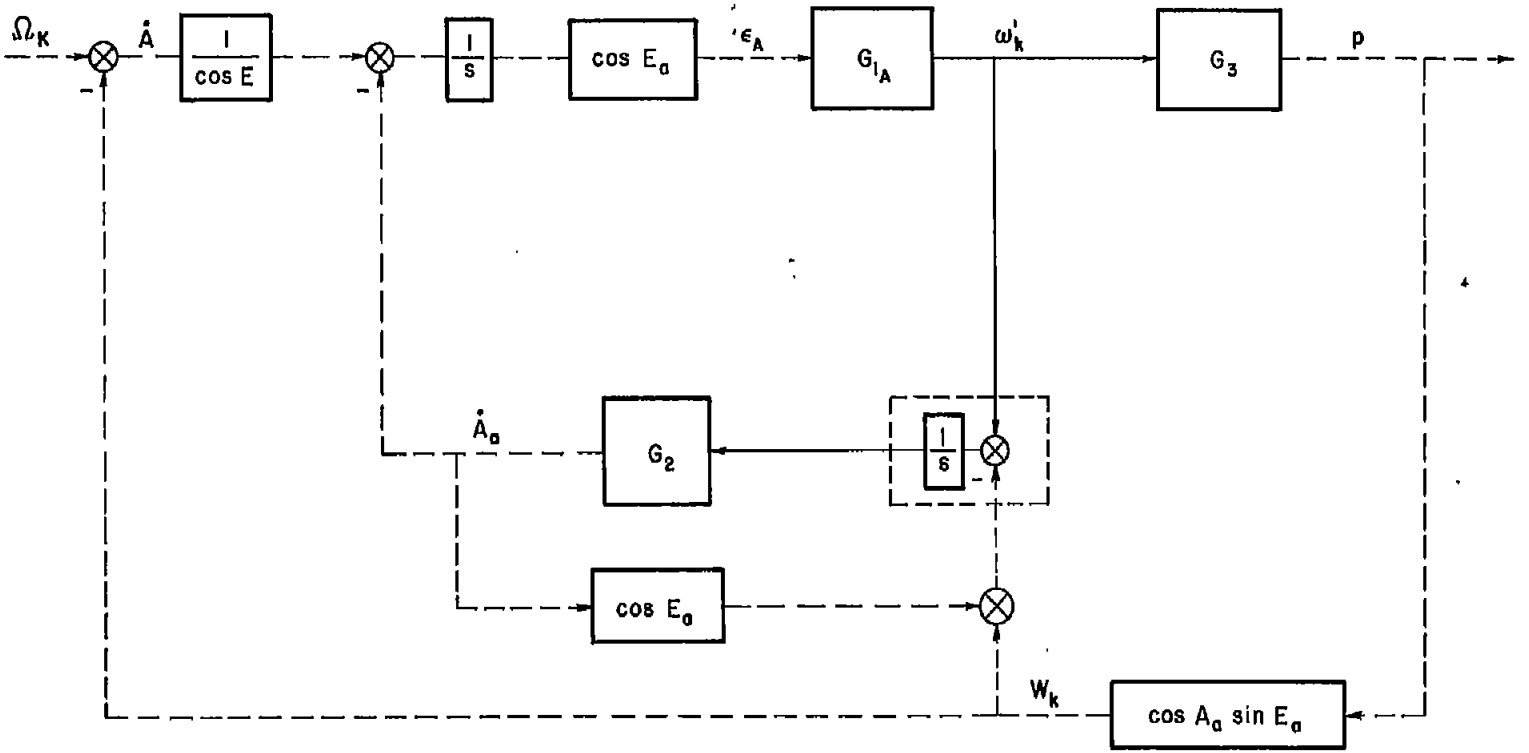

Figure 9.- Block diagram of azimuth channel of radar with airplane rate feedback.

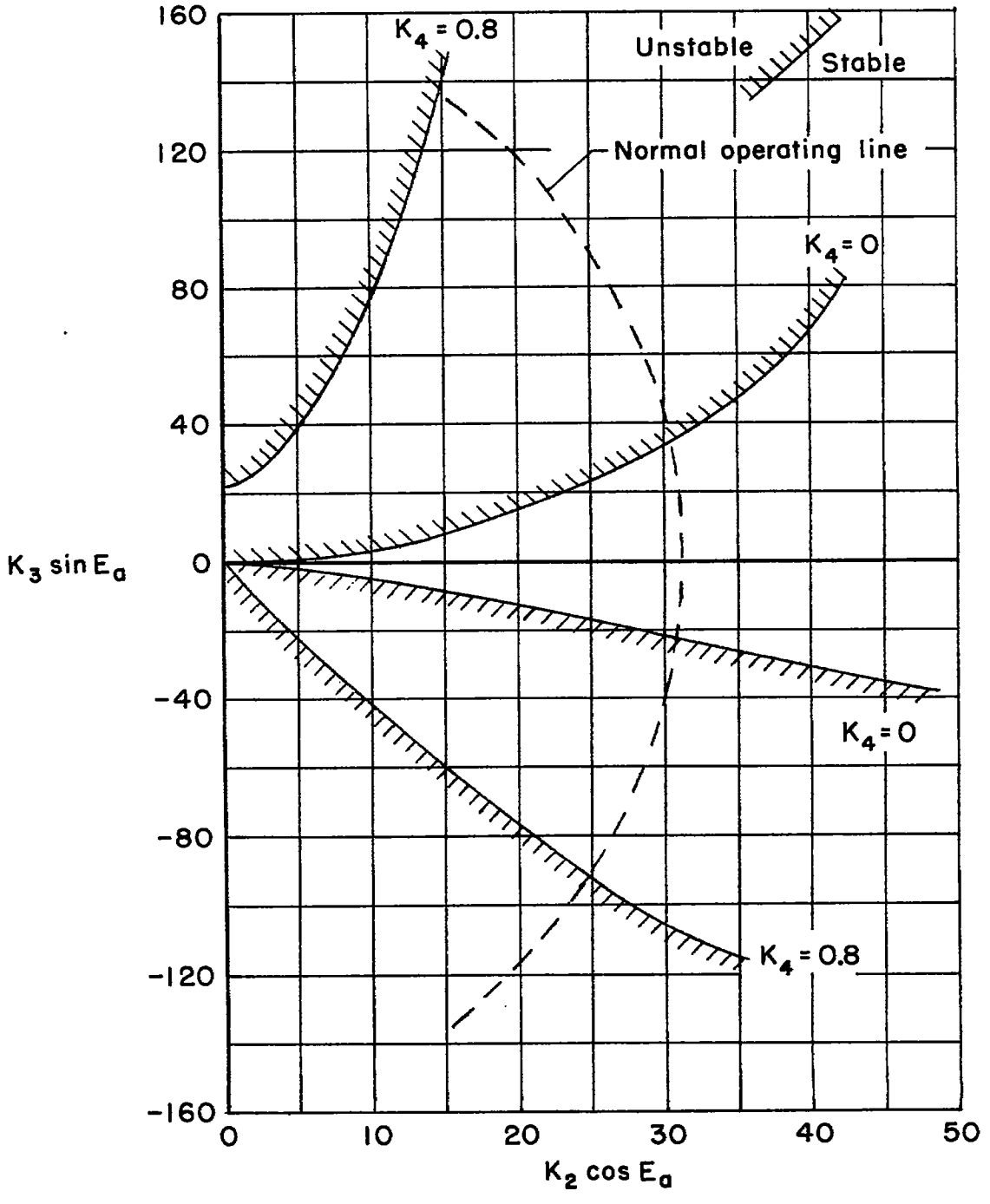

Figure 10.- Approximate stability boundaries for radar with airplane rate feedback; basic and modified systems.

[redacted]

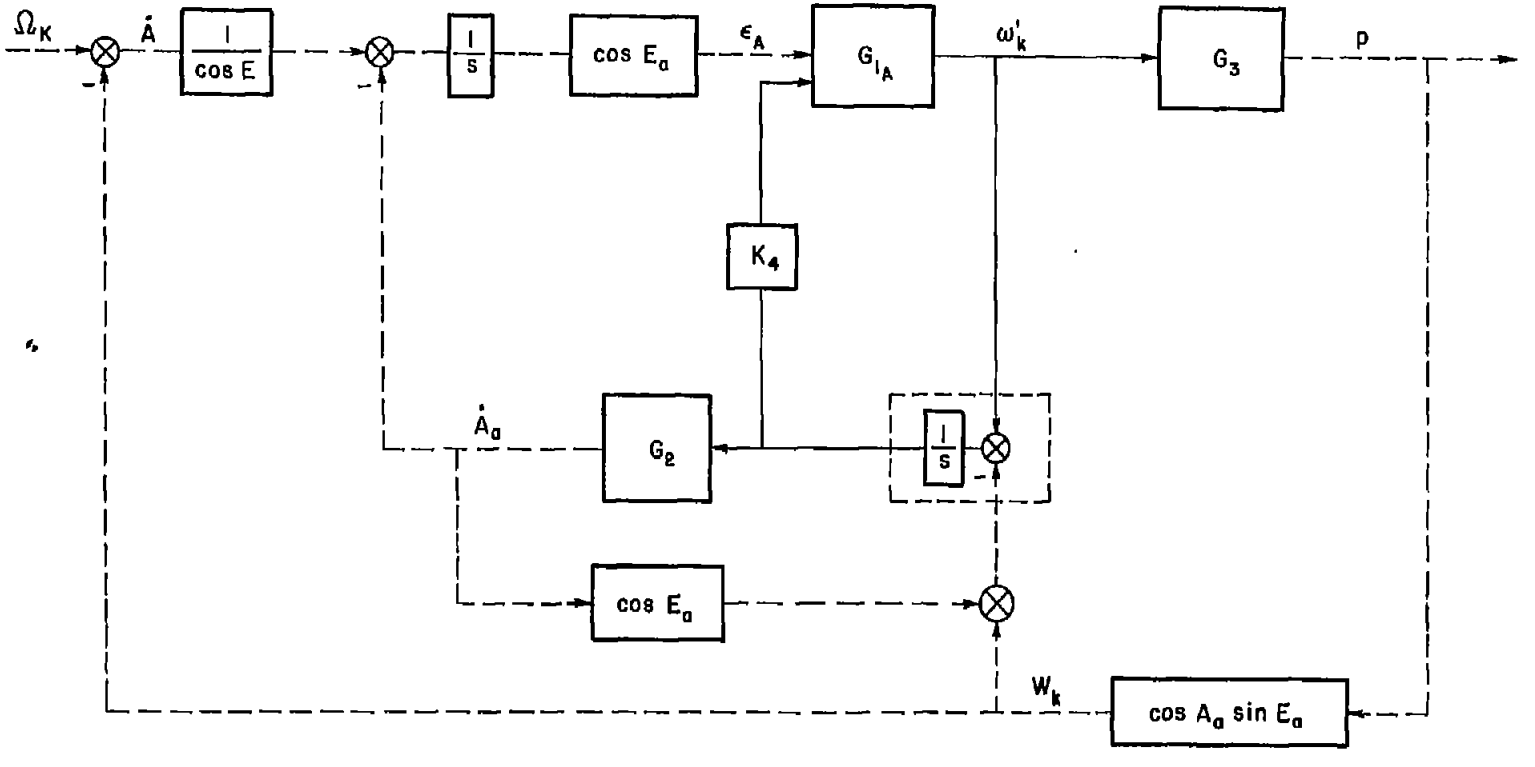

Figure 11.- Block diagram of azimuth channel of modified radar with airplane rate feedback.

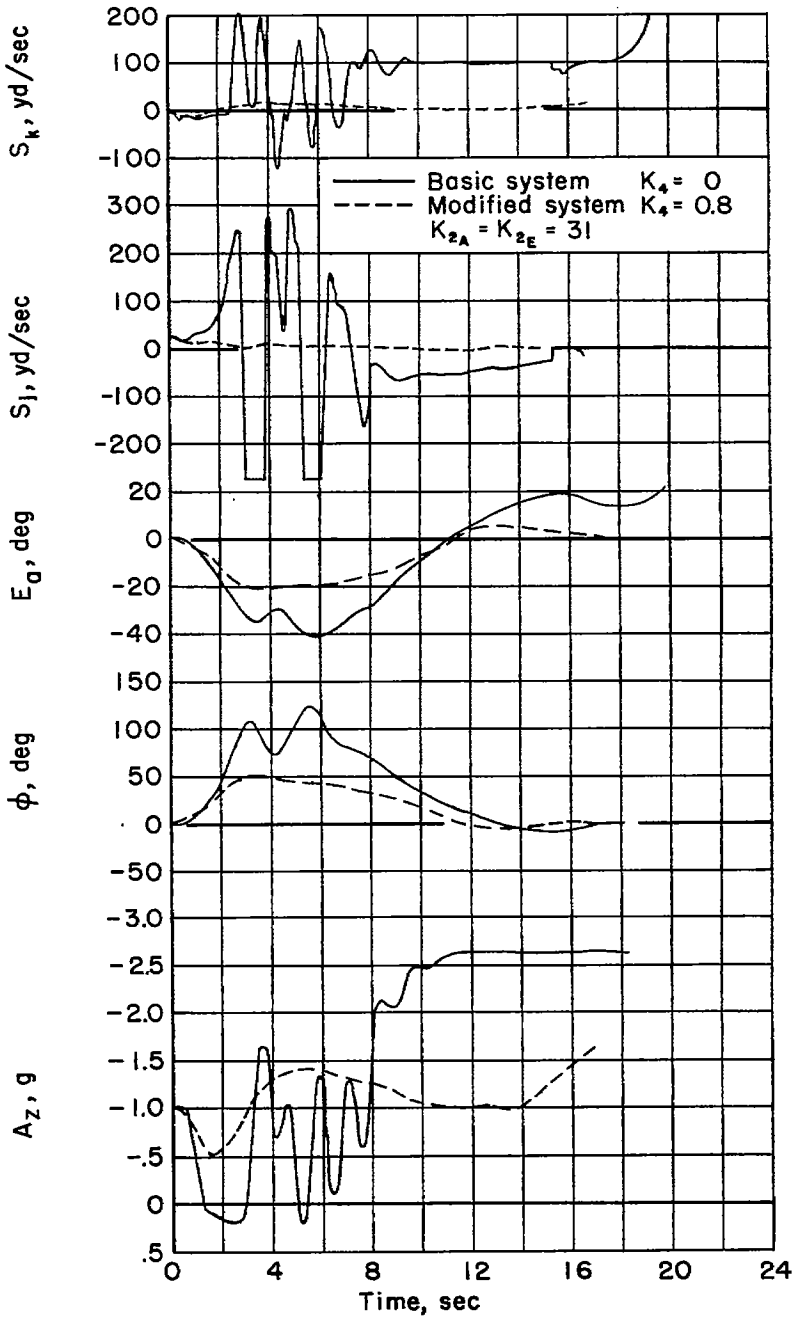

(a) -10° azimuth steering error.

Figure 12.- Analog-computer time history of basic and modified system responses.

[redacted]

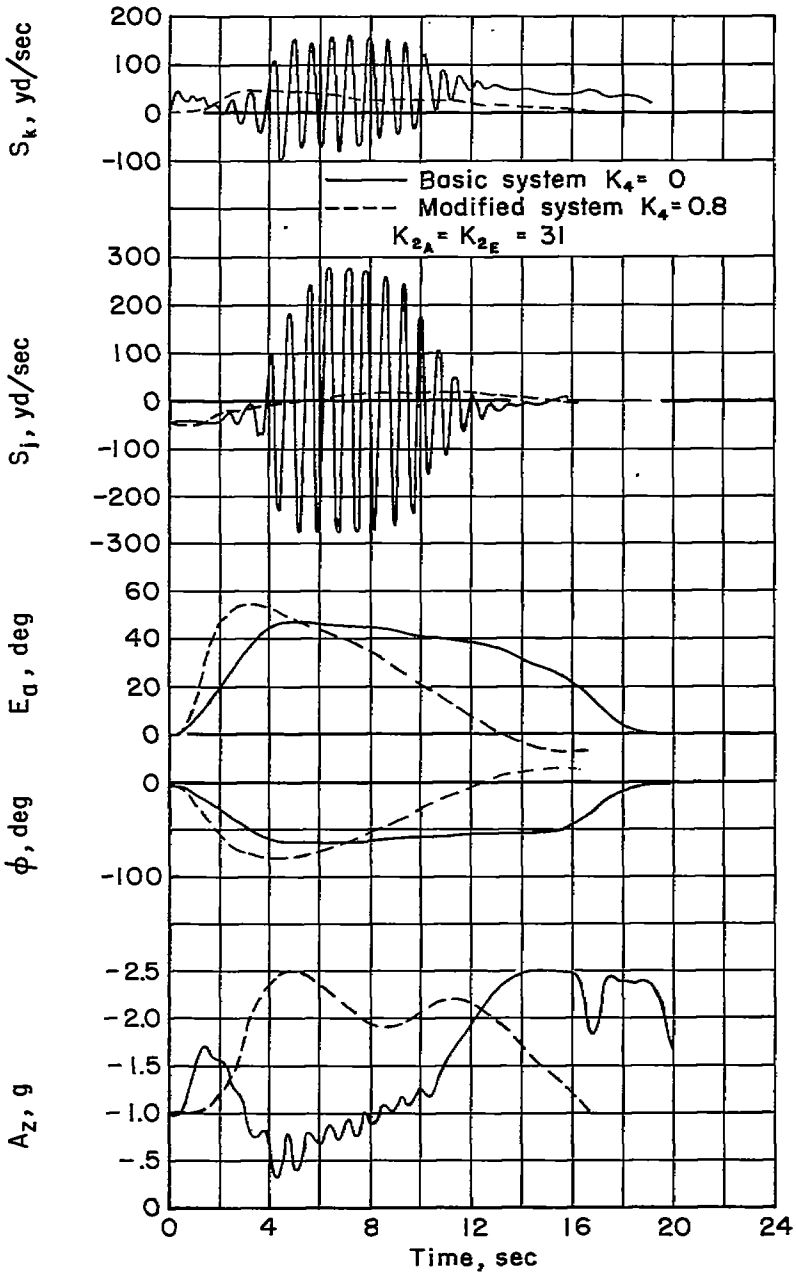

(b) 20° azimuth steering error.

Figure 12.- Concluded.

[redacted]

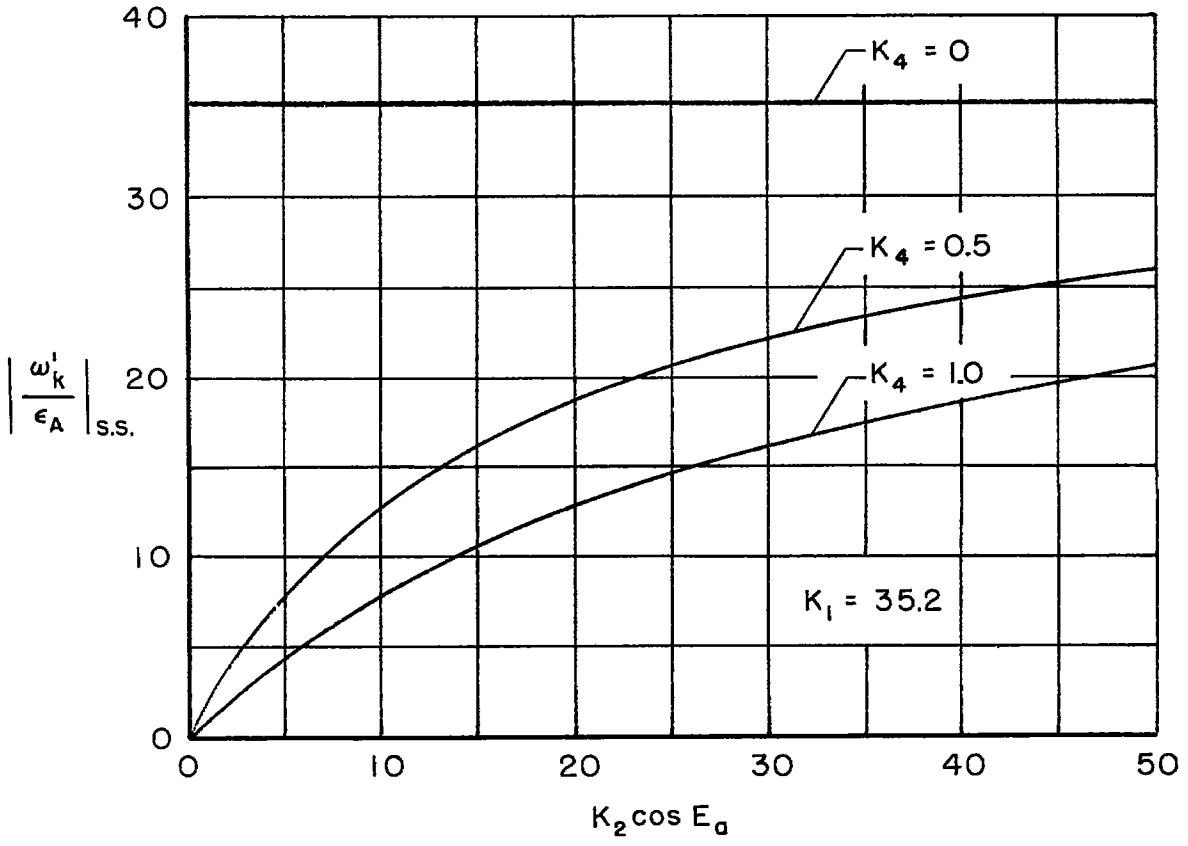

Figure 13.- Steady-state tracking loop gain as a function of effective stabilization loop gain.

[redacted]